Morphologically Selective Synthesis of Nanocrystalline Aluminum Nitride

Joel A. Haber,[†] Patrick C. Gibbons,[‡] and William E. Buhro*,[†]

Departments of Chemistry and Physics, Washington University, St. Louis, Missouri 63130-4899

Received July 9, 1998. Revised Manuscript Received October 1, 1998

Aluminum and N_2 (1 atm) react at 900−1100 °C to give AlN. The nitridation reactions of four types of starting Al powder—nanocrystalline Al of two different origins, and 2-μm and 20-μm Al powders from commercial sources—are described. All four Al powders undergo nitridation to give nanocrystalline AlN; however, only the nanocrystalline Al powders undergo nitridation completely at the low temperatures employed. The nanocrystalline AlN is formed in two principal particle morphologies, equiaxed nanoparticles and nanowhiskers, in relative amounts that depend on reaction conditions and the starting Al powders. Added $AlCl_3$ is an effective promoter of nanowhisker growth. Either AlN morphology may be produced with a high selectivity; samples containing predominately equiaxed nanoparticles or predominately nanowhiskers are readily obtained. The results are consistent with a growth model in which the equiaxed AlN nanoparticles precipitate at or near the surface of coalesced liquid Al droplets, whereas the AlN nanowhiskers grow apart from the Al droplets in a vapor-transport process mediated by $AlCl_3$ and Al subchloride intermediates.

Introduction

We describe the nitridation reactions between N_2 and Al powders having nanometer-to-micrometer-scale initial particle sizes, which give nanocrystalline AlN (nano-AlN). The morphologies of the AlN products depend on the reaction conditions and nature of the starting Al powders. Good selectivities for either equiaxed AlN nanoparticles or AlN nanowhiskers are achieved. Selectivity is most strongly influenced by the presence or absence of $AlCl_3$, a promoter of nanowhisker growth, during nitridation. The growth mechanisms have been characterized; we propose that the equiaxed nanoparticles grow from liquid Al, whereas the nanowhiskers grow from gaseous Al species.

The structural, optical, and refractory applications of AlN have been extensively documented.[1−8] Convenient access to nano-AlN of varying morphology should facilitate its use in electronic packaging[9] and structural composites,[10] which are primary uses of AlN. Nano-AlN sinters to a fully dense ceramic at a significantly lower temperature than does conventional, coarse-grained AlN (1400 vs 1900 °C).[11] Generally, equiaxed particles sinter most efficiently.[12] Whisker, fiber, or platelet morphologies, however, provide better reinforcement in composite materials,[13] and whiskers or fibers have been used to optimize the thermal properties of polymer composites for electronic packaging.[1] Thus, different applications may be imagined for the two principal nano-AlN morphologies described here.

Numerous prior syntheses of nano-AlN have appeared in the literature.[14−24] However, we are unaware of

* To whom correspondence should be addressed. E-mail: buhro@wuchem.wustl.edu.
[†] Department of Chemistry
[‡] Department of Physics

(1) Sheppard, L. M. *Am. Ceram. Soc. Bull.* **1990**, *69*, 1801−1812.
(2) Strite, S.; Morkoc, H. *J. Vac. Sci. Technol. B* **1992**, *10*, 1237−1266.
(3) Baik, Y.; Drew, R. A. L. *Key Eng. Mater.* **1996**, *122−124*, 553−570.
(4) Haussonne, F. J.-M. *Mater. Manuf. Processes* **1995**, *10*, 717−755.
(5) Selvaduray, G.; Sheet, L. *Mater. Sci. Technol.* **1993**, *9*, 463−473.
(6) Mroz, T. J. *Am. Ceram. Soc. Bull.* **1992**, *71*, 782−784.
(7) Marchant, D. D.; Nemecek, T. E. In *Advances in Ceramics*; American Ceramic Society: Westerville, OH, 1989; Vol. 26, pp 19−54.
(8) Balxia, L.; Yinkul, L.; Yi, L. *J. Mater. Chem.* **1993**, *3*, 117−127.
(9) Tummala, R. R. In *Advances in Ceramics*; American Ceramic Society: Westerville, OH, 1989; Vol. 26, pp 3−16.
(10) Huang, J.-L.; Li, C.-H. *J. Mater. Res.* **1994**, *9*, 3153−3159, and references therein.
(11) Baba, K.; Shohata, N.; Yonezawa, M. *Appl. Phys. Lett.* **1989**, *54*, 2309−2311.
(12) Weimer, A. W.; Cochran, G. A.; Eisman, G. A.; Henley, J. P.; Hook, B. D.; Mills, L. K.; Guiton, T. A.; Knudsen, A. K.; Nicholas, N. R.; Volmering, J. E.; Moore, W. G. *J. Am. Ceram. Soc.* **1994**, *77*, 3−18.
(13) Sastry, S. M. L.; Lederick, R. J.; Peng, T. C. *J. Met.*, **1988**, *40*, 11.
(14) Chow, G. M.; Xiao, T. D.; Chen, X.; Gonsalves, K. E. *J. Mater. Res* **1994**, *9*, 168−174.
(15) Wade, T.; Park, J.; Garza, E. G.; Ross, C. B.; Smith, D. M.; Crooks, R. M. *J. Am. Chem. Soc.* **1992**, *114*, 9457−9464.
(16) Bolt, J. D.; Tebbe, F. N. In *Advances in Ceramics*; American Ceramic Society: Westerville, OH, 1989; Vol. 26, pp 69−76.
(17) Ramesh, P. D.; Rao, K. J. *Adv. Mater.* **1995**, *7*, 177−179. Adjaottor, A. A.; Griffin, G. L. *J. Am. Ceram. Soc.* **1992**, *75*, 3209−3214.
(18) Jung, W.-S.; Ahn, S.-K *J. Mater. Chem.* **1994**, *4*, 949−953.
(19) Johnston, G. P.; Muenchausen, R. E.; Smith, D. M.; Foltyn, S. R. *J. Am. Ceram. Soc.* **1992**, 3465−3468.
(20) Pratsinis, S. E.; Wang, G.; Panda, S.; Guiton, T. Weimer, A. W. *J. Mater. Res.* **1995**, *10*, 512−520.
(21) Chen, X.; Gonsalves, K. E. *J. Mater. Res.* **1997**, *12*, 1274−1286.
(22) Li, H.; Yang, H.; Zou, G.; Yu, S. *Adv. Mater.* **1997**, *9*, 156−159.
(23) Janik, J. F.; Wells, R. L.; Coffer, J. L.; St. John, J. V.; Pennington, W. T.; Schimek, G. L. *Chem. Mater.* **1998**, *10*, 1613−1622.
(24) Yu, S.; Dongmei, S.; Sun, H.; Li, H.; Yang, H.; Zou, G. *J. Cryst. Growth* **1998**, *183*, 284−288.

10.1021/cm980481+ CCC: $15.00
Published on Web 11/24/1998

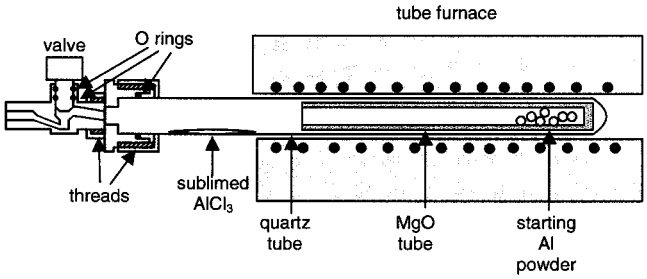

Figure 1. Apparatus used for the nitridation of aluminum powders.

comparable observations of morphological selectivity among them, apart from the preliminary report of these results.[25] To our knowledge, morphological selectivity − the controlled variation of nanocrystallite shape − is rarely achieved in the synthesis of nanocrystalline materials.[26−31]

Experimental Section

General Procedures. All procedures were performed under dry N_2 or in vacuo using glovebox and double-manifold techniques. Pyridine (99.99%, Fisher) was refluxed over KOH for 4 days, distilled, and stored over type 4A sieves. Nanocrystalline aluminum (nano-Al, 40−115 nm mean particle size) was synthesized as described elsewhere.[32] Commercial Al powder (2 μm, 99%, Strem; 20 μm, 99%, Aldrich) was stored under N_2 and used as received.

Synthesis of Nano-AlN. The nitridations were performed using the apparatus depicted in Figure 1. Nitridations were conducted in MgO tubes closed at one end (Ozark Technical Ceramics) that were degassed at 750−1100 °C under dynamic vacuum for 8−10 h before the initial use and subsequently stored in a N_2-filled glovebox. In some cases the nano-AlN product was contaminated with MgO and/or with $MgAl_2O_4$ when new MgO tubes were used, but after several synthetic runs a protective layer of AlN accumulated in the tubes, which prevented contamination.

For a typical complete nitridation, the MgO tube was loaded with 0.2−0.6 g of nano-Al (2-μm or 20-μm Al powder) and inserted into a fused-silica tube sealed on one end and fitted with an Ultratorr valve assembly on the other end. The assembly was removed from the glovebox and placed into a tube furnace. After appropriate purging of the connecting lines the valve was opened to N_2 (1 atm). The sample was heated to 900−1100 °C for 10 h using a heating rate of 20, 50, or 100 °C/min to produce nano-AlN. Maximum heating rates were obtained by inserting the reaction tube into a furnace preheated to 900−1100 °C. The nano-AlN powder was then collected from the tube by spatula. In runs in which additives were employed, the additives were premixed with the nano-Al in a ceramic mortar and pestle.

Yields were typically 0.2−0.9 g (50−96% yield); however, >100% yields were sometimes calculated because of breakdown and inclusion of the AlN accumulated in the tube during previous reactions. Runs conducted with large amounts of added $AlCl_3$ (such as 93 wt %) were particularly susceptible to this problem.

Large-scale reactions were conducted using 2 g of Al. Elemental analysis (Galbraith Laboratories with airless handling) of nano-AlN prepared by heating 2.0 g of nano-Al (from eq 2; see Results) under N_2 at 1100 °C for 10 h found (wt %) Al, 63.5; N, 32.2; Ti, 0.32; C, <0.5; Mg, <0.06; O, <4.6 (by difference). Analysis of nano-AlN prepared by mixing 2.05 g of the same nano-Al with 0.21 g $AlCl_3$ (9.3 wt %) and reacting it identically to the previous sample found (wt %) Al, 66.4; N, 31.9; Cl, 0.27; Ti, <0.09; C, 0.56; Mg, <0.09; O, <0.9 (by difference); calcd (wt %) Al, 65.8, N, 34.2.

Partial nitridation reactions were performed by heating 0.3−0.7 g of Al or Al/$AlCl_3$ mixtures to 1000 °C at 20 or 50 °C/min. The apparatus was held at 1000 °C for 15 min and then removed from the furnace to cool rapidly. The size ranges of partially reacted droplets from different initial Al sizes and heating rates were as follows: nano-Al, 20 °C/min, 5−80 μm; nano-Al, 50 °C/min, 5−15 μm, 2 μm Al, 50 °C/min, 1−100 μm; 20 μm Al, 20 °C/min, 5−1500 μm; 20 μm Al, 50 °C/min, 1−300 μm. The size range of partially reacted droplets from different initial Al sizes and heating rates with $AlCl_3$ added were as follows: nano-Al, 20 °C/min, 5−40 μm; nano-Al, 50 °C/min, 3−20 μm, 2 μm Al, 50 °C/min, 2−30 μm; 20 μm Al, 20 °C/min, 3−100 μm; 20 μm Al, 50 °C/min, 1−100 μm.

Transmission electron microscopy (TEM) was performed on a JEOL 2000 FX instrument operating at 200 keV. Suspension of 10−50 mg of powder in 10−50 mL of dry pyridine by sonication for 15−420 min in an ultrasonic cleaning bath was the preferred method of TEM sample preparation. Powders that were loosely agglomerated suspended rapidly, while heavily aggregated powders required sonication for extended periods. While sonication continued, a few drops of the suspension were removed by syringe and placed on a holey-carbon-coated Ni TEM grid in air. The grid was immediately placed into a tightly capped vial with 2−5 drops of the pyridine suspension and loaded directly into the TEM specimen airlock while still wet with pyridine. This method proved quite effective at limiting oxidation of even partially reacted samples. Ni TEM grids were generally employed because Cu grids reacted with whisker-rich samples. Large pale-green whiskers grew on the Cu grids when whisker-rich suspensions were placed on them; in some cases the grid was totally covered, preventing TEM analysis. According to EDS, the large pale-green whiskers contained large amounts of C, Cu, and O and smaller amounts of N and Al.

Scanning electron microscopy (SEM) was performed on a Hitachi S-4500 field-emission instrument. SEM specimens were prepared by dusting powders on carbon tape on Al stubs in the N_2-filled glovebox. The stubs were sealed in tightly capped vials, and SEM studies were performed immediately after removing the vials from the glovebox. The stubs were rapidly transferred from the vials to the SEM sample-exchange chamber to limit air exposure to less than 1 min.

Energy dispersive spectroscopy (EDS) with light-element detection was performed in conjunction with TEM and SEM using Noran Instruments Voyager II X-ray Quantitative Microanalysis Systems with Digital Imaging.

X-ray Diffraction (XRD) Procedures. XRD patterns were obtained using a Rigaku vertical powder diffractometer with Cu Kα (λ = 1.541845 Å) radiation and Materials Data Incorporated (MDI) automation and software. The XRD samples (1.5 × 2 cm smear mounts) were prepared in an N_2-filled glovebox and coated with a thin film of polyvinyltoluene (PVT) to minimize air exposure. The PVT film was applied by dripping a toluene solution of PVT onto the prepared XRD slide and evaporating to dryness. For each AlN sample the MDI software was used to correct the baseline, subtract the Kα2 peaks, and calculate the coherence lengths for the {100}, {002}, {101}, {102}, {110}, {103}, {200}, {112}, {201}, and {004} peaks. The mean of the coherence lengths calculated for each peak was taken to be the mean coherence length of the sample, and the standard deviation in the coherence lengths for the different peaks was used as a measure of the error in the mean coherence length.

(25) Haber, J. A.; Gibbons, P. C.; Buhro, W. E. *J. Am. Chem. Soc.* **1997**, *119*, 5455−5456.
(26) Ahmadi, T. S.; Wang, Z. L.; Green, T. C.; Henglein, A.; El-Sayed, M. A. *Science* **1996**, *272*, 1924−1926.
(27) Tanori, J.; Pileni, M. P. *Adv. Mater.* **1995**, *7*, 862−864.
(28) Petroski, J. M.; Wang, Z. L.; Green, T. C.; El-Sayed, M. A. *J. Phys. Chem. B*, **1998**, *102*, 3316−3320.
(29) Pileni, M. P. *Ber. Bunsen-Ges. Phys. Chem.* **1997**, *101*, 1578−1587.
(30) Cain, J. L.; Nikles, D. E. *IEEE Trans. Magn.* **1997**, *33*, 3718−3720.
(31) Tanori, J.; Pileni, M. P. *Langmuir* **1997**, *13*, 639−646.
(32) Haber, J. A.; Buhro, W. E. *J. Am. Chem. Soc* **1998**, *120*, 10847−10855.

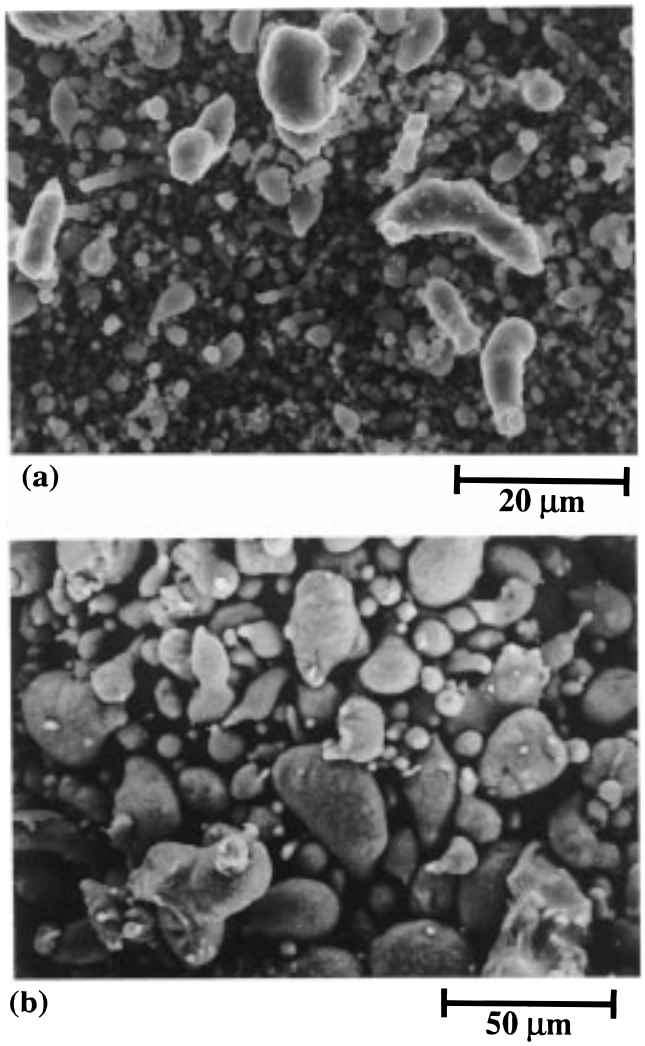

Figure 2. SEM micrographs of the commercial Al powders: (a) 2-μm Al and (b) 20-μm Al.

Results

Conversion of Al to AlN. Four types of starting Al powder were studied. Two were 2-and 20-μm commercial powders. The 2-μm powder consisted of particles having diameters of 0.5−20 μm (Figure 2a). The 20-μm powder consisted of particles having diameters of 2−75 μm (Figure 2b). Two starting Al powders were nano-Al samples prepared by solution-based syntheses.[32] These samples were obtained from eqs 1 and 2 and are hereafter referred to as eq-1 Al and eq-2 Al. A brief description of eq-1 and eq-2 Al is given to illuminate the nitridation results that follow.

$$3LiAlH_4 + AlCl_3 \xrightarrow[164\ °C]{1,3,5\text{-}Me_3C_6H_3} 4\text{nano-Al} + 3LiCl + 6H_2 \quad (1)$$

$$H_3Al(NMe_2Et) \xrightarrow[\substack{0-1.2\ \text{mol \% Ti(O-}i\text{-Pr)}_4\\ \text{ca. 164 °C}}]{1,3,5\text{-}Me_3C_6H_3} \text{nano-Al} + NMe_2Et + {}^3/_2H_2 \quad (2)$$

Eq-1 Al was generated by reduction of $AlCl_3$ with $LiAlH_4$ and was washed with MeOH to remove the LiCl byproduct.[32] The Al crystallite sizes were 160 ± 50 nm as determined by XRD, TEM, and SEM measurements, and the crystallites were highly agglomerated. Elemental analysis established that eq-1 Al was only 87 wt % Al and contained residual aluminum chloride (equivalent to ca. 4 wt %).

Eq-2 Al was generated by thermal decomposition of $H_3Al(NMe_2Et)$, with or without Ti(O-*i*-Pr)$_4$ added as a decomposition catalyst, and did not require washing for purification.[32]

The mean coherence lengths and degree of agglomeration in eq-2 Al depended upon the catalyst concentration. Powders having mean coherence lengths of 60−70 nm were highly aggregated, like eq-1 Al. Powders having larger mean coherence lengths of 70−100 nm contained large nonagglomerated fractions. Eq-2 Al was ≥99 wt % Al.

The four types of starting A—2-μm, 20-μm, eq-1, and eq-2 Al—underwent nitridation according to eq 3 (900−1100 °C). The characteristics of the AlN produced depended on the type of Al used.

$$Al + {}^1/_2N_2 \rightarrow AlN \quad (3)$$

The morphological distribution in the AlN obtained from eq-1 Al differed from those obtained from the other types of Al. All four types of starting Al gave AlN crystallites with mean dimensions in the nanometer regime. Both eq-1 and eq-2 Al gave nano-AlN having coherence lengths of 20−30 nm (eq 3, 1100 °C). The AlN usually contained no impurities detectable by XRD, apart from traces of MgO and $MgAl_2O_4$ when new MgO reaction tubes were employed. TEM images of the nano-AlN derived from eq-1 Al showed that it contained a mixture of equiaxed (Figure 3a) and whisker (Figure 3b) nanoparticle morphologies. In some cases a small fraction of platelets was also observed. In contrast, nitridation of eq-2 or 2-μm Al produced equiaxed nano-AlN particles containing very few whiskers or platelets. The results suggested that eq-1 Al contained an adventitious whisker-growth promoter that was absent in the other Al powders (see below).

The extent of the nitridation reaction (eq 3) depended on the particle sizes in the starting Al. The nanosized eq-1 and eq-2 Al powders reacted more completely than did the 2- and 20-μm Al powders. Small amounts of unreacted Al were detected by XRD with all four starting Al powders when they were heated under N_2 at 1100 °C for only 30 min. When the heating period was extended to ≥2 h, the Al reflections were no longer detected in any of the four cases. However, EDS analyses (conducted in the TEM) of the nitridation product from 2-μm Al (with and without 10−13 wt % $AlCl_3$ added; see below) revealed excess Al. Similar EDS analyses of the nitridation products from eq-1 and eq-2 Al found no excess Al. Note that the nano-Al powders from eqs 1 and 2 did not contain the >5 μm particles that constituted a significant fraction of the 2-μm powders. These larger particles likely became deactivated toward complete nitridation when coated by AlN product (see below). Although the nano-Al particles used here were assembled into quite dense 1−3-μm aggregates, the nanoporosity and large grain-boundary-volume fraction in the aggregates apparently provided sufficient pathways for N and Al diffusion to sustain the nitridation process to completion.

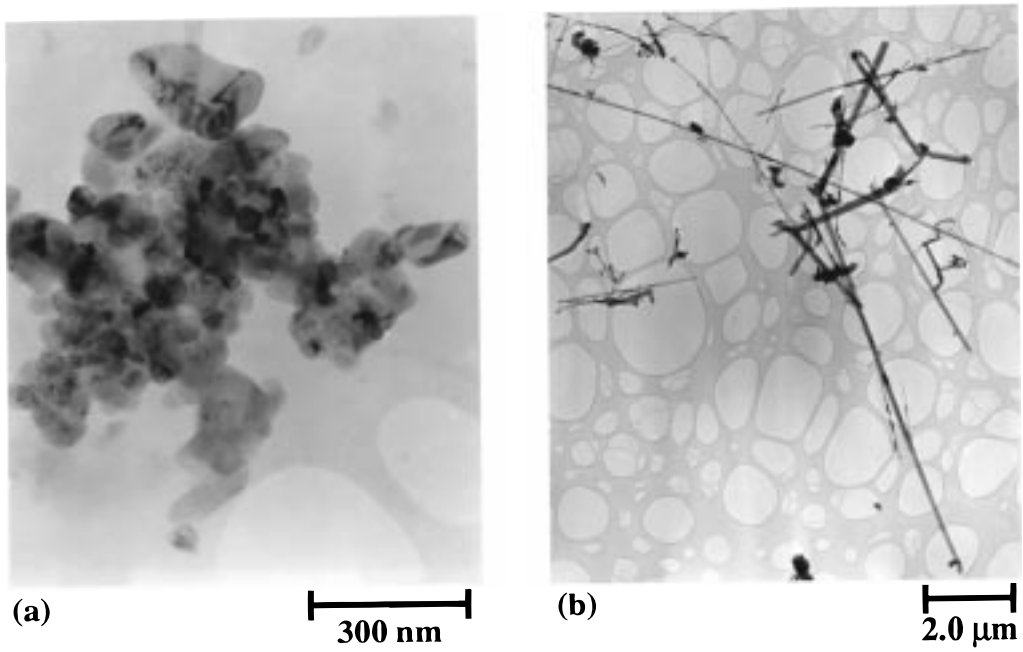

Figure 3. Typical AlN morphologies obtained by nitridation of Al powders, in this case of eq-1 nano-Al: (a) aggregate of equiaxed nanoparticles and (b) nanowhiskers.

Promotion of Whisker Growth by $AlCl_3$. As noted above, we surmised that eq-1 Al may have contained an adventitious whisker-growth promoter. To test this possibility, we added several potential promoters that may have been adventitiously present in eq-1 Al to eq-2 Al and then conducted nitridation trials. Addition of the potential fluxes Li_2O (15 wt %), $LiAlO_2$ (6 or 74 wt %), or $LiAl_5O_8$ (6 wt %) or the Cl_2 source $SbCl_5$ (71 or 94 wt %) to eq-2 Al exerted minimal effects on whisker yields or completeness of nitridation. Eq-2 Al to which LiCl (12 wt %) was added gave incomplete reaction. However, addition of $AlCl_3$ (9−12 wt %) to eq-2 Al produced nano-AlN containing a whisker fraction comparable to that obtained from eq-1 Al. Although addition of $AlCl_3$ (10−12 wt %) to 2-μm Al also greatly increased the nanowhisker fraction, the fraction was lower than that obtained from comparably treated eq-2 Al.

That $AlCl_3$ played a role in whisker formation was further evidenced by the change in the distribution of particle morphologies with increasing $AlCl_3$ content. When no $AlCl_3$ was added to eq-2 Al powders, only a small whisker fraction was obtained (Figure 4a). When 9−12 wt % of $AlCl_3$ was added, a significant fraction of straight nanowhiskers (ca. 50%) was obtained (Figure 4b), while addition of 93 wt % $AlCl_3$ produced a very large fraction (ca. 90%) of whiskers and branched and comblike crystallites (Figure 4c). A large fraction of whiskers was also observed by SEM (Figure 4d), which indicated that the high whisker fraction was not an artifact of TEM sample preparation. Other unusual morphologies were obtained in addition to the branched and comblike crystallites in the cases having the highest whisker fractions; these are discussed below (see Dependence of AlN morphologies on Reaction Variables).

Thus, $AlCl_3$ was identified as a whisker-growth promoter. Nitridation of eq-1 Al, which contained the equivalent of ca. 4 wt % residual $AlCl_3$, produced a whisker yield comparable to that produced from eq-2 Al to which 9−12 wt % $AlCl_3$ was added. The greater efficiency of the $AlCl_3$ present in eq-1 Al was likely due to more intimate mixing than was achieved by grinding eq-2 Al and $AlCl_3$ in a mortar and pestle.

However, eq-1 Al contained C and O impurity levels that were an order of magnitude greater than those present in eq-2 Al. Nitridation of eq-1 Al containing these higher impurity levels yielded lower purity nano-AlN than was obtained by nitridation of the purer eq-2 Al. We believe that Al purity and the manner of $AlCl_3$ incorporation were the only significant factors that differentiated the nitridation results of the eq-1 and eq-2 Al powders.

In addition to improving the whisker yield, $AlCl_3$ reduced the total concentrations of O and Ti impurities in the AlN produced from eq-2 Al. The nano-AlN obtained from eq-2 Al without added $AlCl_3$ contained 0.32 wt % Ti and ≤4.6 wt % O, whereas nano-AlN obtained from the same batch of eq-2 Al with 9.2 wt % $AlCl_3$ contained <0.09 wt % Ti and <0.9 wt % O (see the Experimental Section). $AlCl_3$ apparently transported Ti and O from the reaction vessel as volatile compounds.

We found that the whiskers and fine equiaxed AlN particles could be separated from the platelets, coarse particles, and aggregates. Separation was accomplished by suspending the nano-AlN powders (ca. 0.1−0.3 g) in pyridine (50−150 mL) with sonication and allowing the coarse particles and aggregates to settle (ca. 3−8 h). The supernatant was enriched in whiskers and fine particles. Because the whiskers contained less oxygen than did the aggregates of equiaxed particles (see below), this separation was also a means of increasing the purity of the AlN.

AlN Nanowhisker Characterization. The AlN nanowhiskers ranged from 20 to 500 nm in diameter and to >30 μm in length, with aspect ratios (length/diameter) ranging from 5 to >250. Most whiskers were 20−100 nm in diameter, with aspect ratios of 20−100.

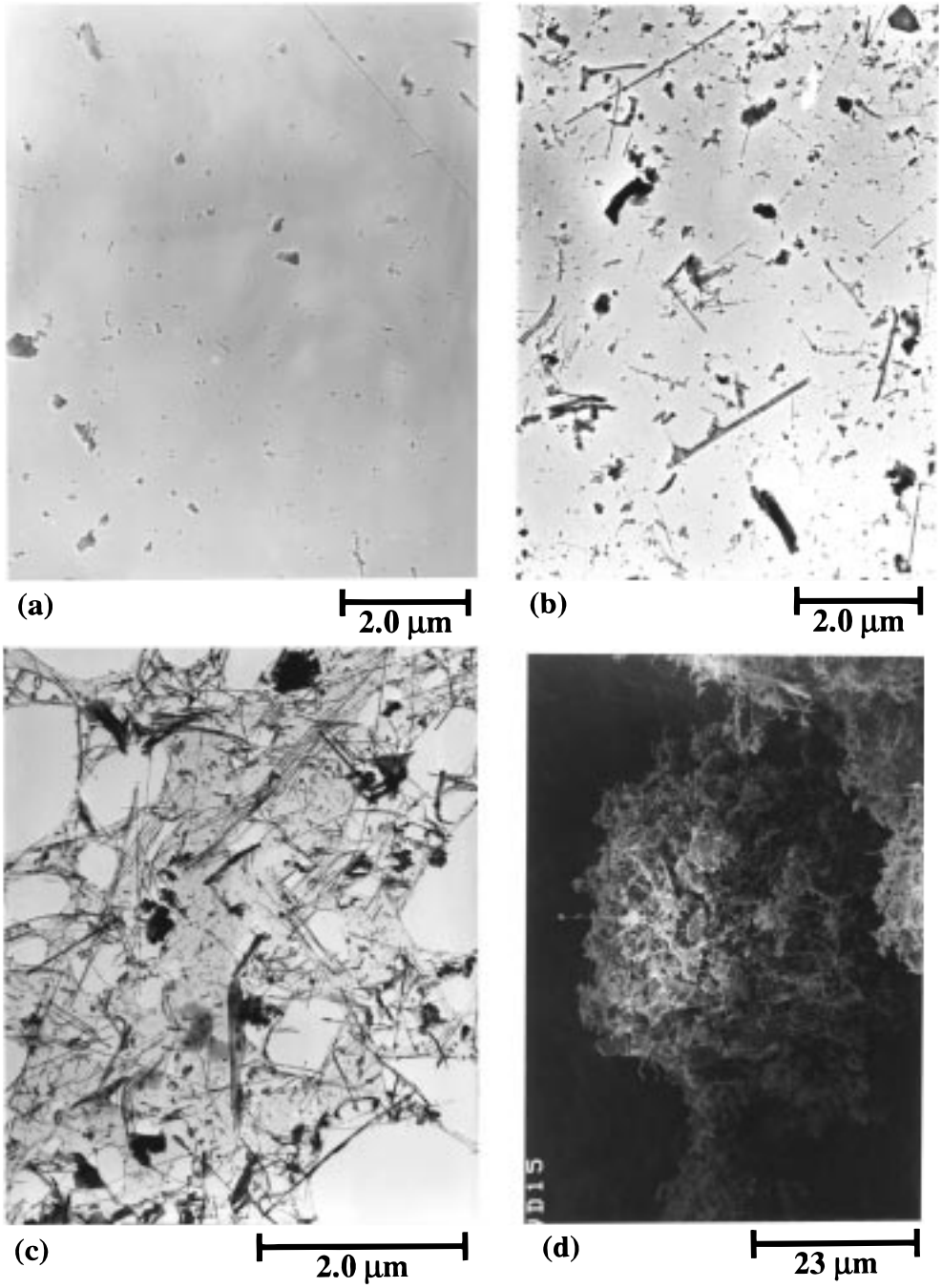

Figure 4. Images showing increasing AlN nanowhisker fractions upon eq-2 Al nitridation in the presence of increasing amounts of $AlCl_3$: (a) with 0 wt % $AlCl_3$, (b) with 10 wt % $AlCl_3$, (c) with 93 wt % $AlCl_3$ (TEM image), and (d) with 93 wt % $AlCl_3$ (SEM image).

While almost all whiskers were straight with uniform diameter over the length of the whisker, unusual morphologies were also observed, including bent, curved, ax-shaped, hexagonal cone, and hollow tube. The whiskers were found to be single crystals by selected-area electron diffraction conducted in the TEM and indexed to the common (hexagonal) wurtzite structure.

Several growth directions for AlN whiskers have been reported previously, including normal to the densely packed (001), (100), and (101) planes.[33−35] We found two common growth directions in our samples. The crystallographic orientation of the long axis of several whiskers was determined using electron-diffraction patterns of tilted and rotated whiskers. In most cases indexing was simplified by the appearance of the forbidden 001 spots, which have a unique *d* spacing, by dynamical diffraction.[36] That the forbidden 001 peaks were produced by dynamical diffraction was confirmed by their absence in patterns for zones in which dynamical diffraction would not produce them. In four whiskers having

(33) Itoh, H.; Morikawa, H.; Sugiyama, K. *J. Cryst. Growth* **1989**, *94*, 387−391.
(34) Drum, C. M.; Mitchell, J. W. *Appl. Phys. Lett.* **1964**, *4*, 164−165.
(35) Caceres, P. G.; Schmid, H. K. *J. Am. Ceram. Soc.* **1994**, *77*, 977−983.
(36) Williams, D. B.; Carter, C. B. *Transmission Electron Microscopy*; Plenum: New York, 1996; Vol. II, p 247.

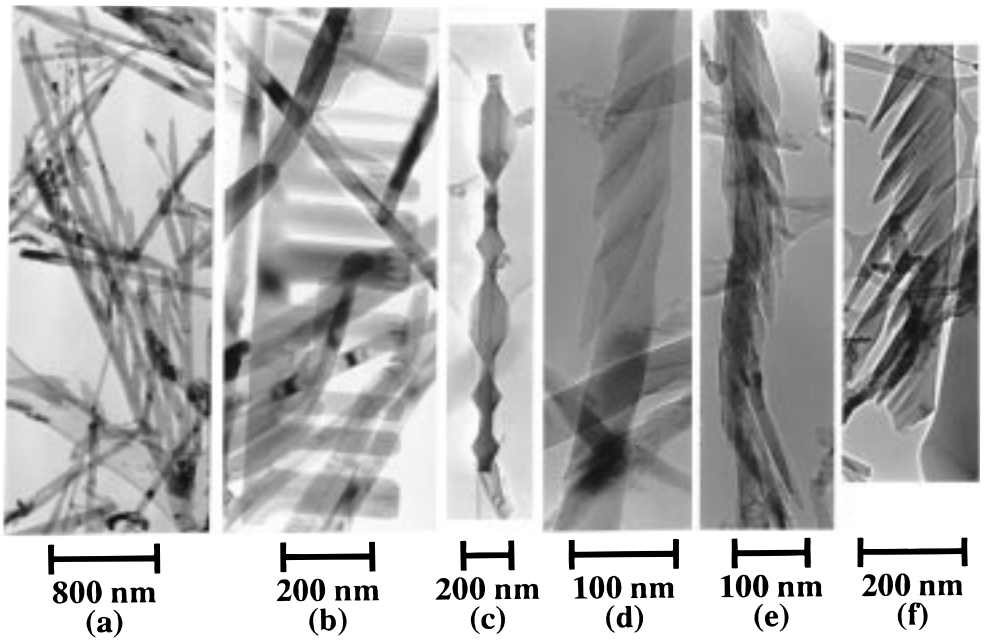

Figure 5. Unusual AlN crystallite morphologies obtained upon Al nitridation using rapid heating rates in the presence of added $AlCl_3$: (a) branched crystallite, (b) comblike crystallite, (c) whisker decorated with protruding platelets, and (d and e) scale-decorated crystallites.

diameters >200 nm, two with hexagonal cross sections, the whisker axes appeared to be parallel to the *c* direction of the wurtzite unit cell (that is, growth was normal to the (001) planes). In two whiskers having diameters <200 nm the whisker axis was normal to the (100) planes (that is, the growth direction was perpendicular to the *c* direction). A T-shaped crystallite with a diameter of 120 nm grew in both directions; the long trunk of the T was parallel to the *c* direction while the top grew normal to the (100) planes (which is normal to the *c* direction). A correlation between whisker diameter and growth direction may exist.

EDS analyses established that the whiskers contained lower levels of O than did the aggregates of equiaxed particles. We attempted to conduct standardized EDS measurements but encountered fairly large instrumental uncertainties associated with the focusing of the electron beam to small spot sizes. Consequently, the EDS results are only semiquantitative. The aggregates of equiaxed AlN particles from nitridation of eq-1 Al had ≥4 times the O content of the AlN whiskers and platelets from the same synthesis. The difference in the O content of the aggregates of equiaxed AlN particles and whiskers from nitridation of eq-2 Al was much less (≤2 times). Recall that eq-2 Al was of significantly higher purity than was eq-1 Al. The greater purity of the whiskers was consistent with a vapor−solid growth mechanism in which the AlN whiskers grew from volatilized gaseous nutrients, while the equiaxed AlN particles grew from Al(l) droplets in which the impurities remained concentrated. In general whiskers contained more oxygen than did platelets, and fine whiskers contained more oxygen than did large whiskers, suggesting that surface hydrolysis was a primary source of the O detected in the whiskers.

Although the EDS data did not provide a precise measure of the absolute O content of the AlN nanowhiskers, we were able to estimate the O content by analyzing contrast bands in TEM images of the nanowhiskers. Characteristic contrast bands arise from two-dimensional defects in AlN crystals at O concentrations of ≥0.75 atom %.[35,37,38] Approximately half our nanowhiskers contained these contrast bands and half were free of them. Consequently, we estimated that the nanowhiskers contained a mean O content of ca. 0.75 atom %, or 0.58 wt %. This value is consistent with the value of <0.9 wt % O obtained from bulk analyses of the purest AlN powders (which were mixtures of all particle morphologies).

Dependence of AlN Morphologies on Reaction Variables. The distributions of AlN particle morphologies depended on the extent of nitridation, the initial particle sizes in the starting Al powders, and heating rate. Conditions expected to enhance the rate of Al evaporation generally gave larger AlN nanowhisker fractions, supporting a nanowhisker growth mechanism involving gaseous nutrient species.

We found that the AlN morphological distribution varied over the course of the nitridation process. For all four types of starting Al powder, nitridation gave at least some AlN nanowhiskers, even when no $AlCl_3$ was added. The suspendable portions of eq-2, 2-μm, and 20-μm Al powders that were nitrided without added $AlCl_3$ and to only partial completion were whisker rich. The nonsuspendable portions of these samples contained large (>2 μm), dense Al/AlN aggregates. Complete nitridation greatly decreased the whisker fractions within the suspendable portions. The results indicated that in the absence of the $AlCl_3$ whisker-growth promoter, most of the whiskers formed early in the nitridation process and that the unreacted Al held the equiaxed AlN particles in Al/AlN aggregates until the Al was consumed. We surmised that Al evaporation

(37) Harris, J. H.; Youngman, R. A.; Teller, R. G. *J. Mater. Res.* **1990**, *5*, 1763−1773.
(38) Westwood, A. D.; Youngman, R. A.; McCartney, M. R.; Cormac, A. N.; Notis, M. R. *J. Mater. Res.* **1995**, *10*, 2573−2585.

supporting nanowhisker growth was rapid from the initially small Al particles, but as the Al melted and coalesced into large droplets and/or aggregates, the rate of Al evaporation and hence the rate of nanowhisker growth was diminished.

The initial Al particle size and rate of heating during nitridation affected the morphological distribution of the AlN produced when $AlCl_3$ was added. As noted above, lower whisker fractions were obtained using 2-μm Al than were obtained using eq-2 (nano-)Al with heating rates of 20 or 50 °C/min. However, 2-μm Al produced a much larger yield of nanowhiskers at the increased heating rate of 100 °C/min than was obtained with lower heating rates. The larger Al surface area provided by the smaller Al particles should have enhanced the rate of Al evaporation. We found that faster heating rates did preserve a larger Al surface area by minimizing coalescence of the molten Al particles (see below). Smaller initial particle sizes and more-rapid heating rates would produce the observed increased nanowhisker yield if nanowhiskers grow from gaseous nutrients, as we propose.

The fastest heating rates (≥100 °C/min), addition of large amounts of $AlCl_3$, or use of nonagglomerated eq-2 (nano-)Al produced large fractions of unusual crystallite morphologies. These included branched, comblike, and scale-decorated whiskers (Figure 5) and twisted, polycrystalline fibers (Figure 6). In contrast, 2-μm Al continued to produce straight AlN nanowhiskers under these conditions. The formation of the unusual morphologies at the highest nutrient vapor concentrations is consistent with a vapor−solid growth mechanism (see the Discussion section).

The highest selectivities for AlN nanowhiskers and, alternatively, for equiaxed particles were obtained under the following conditions. Nitridation of 2-μm Al in the presence of 10 wt % $AlCl_3$ using a rapid heating rate (insertion of reaction apparatus into an oven preheated to 1100 °C) gave the highest yield of straight, well-formed nanowhiskers. However, the average size of these whiskers was slightly larger than those produced from the eq-1 or eq-2 nano-Al powders. The eq-2 Al was not the best nanowhisker precursor material, because its nitridation produced significant amounts of the unusual morphologies noted above. Alternatively, nitridation of eq-2 Al using a heating rate of 20 °C/min and *no* $AlCl_3$ gave the highest yield of equiaxed nano-AlN particles.

Intermediate Microstructures in Partial-Conversion Experiments. Partially reacted Al powders were microscopically examined to help elucidate the mechanisms of whisker and equiaxed-particle formation. Reaction variables were shown above to influence the morphologies of the AlN product. Here we found that the presence of $AlCl_3$, the initial Al particle size, and the heating rate also influenced the size and morphology of incompletely reacted Al droplets. The results suggested that the equiaxed AlN particles grew upon and in close proximity to coalesced Al droplets, whereas the AlN nanowhiskers grew remotely using Al transported from the droplets.

With all starting Al powders, the Al particle size distribution in the partially reacted samples was shifted to be larger than the initial sizes. In all cases Al

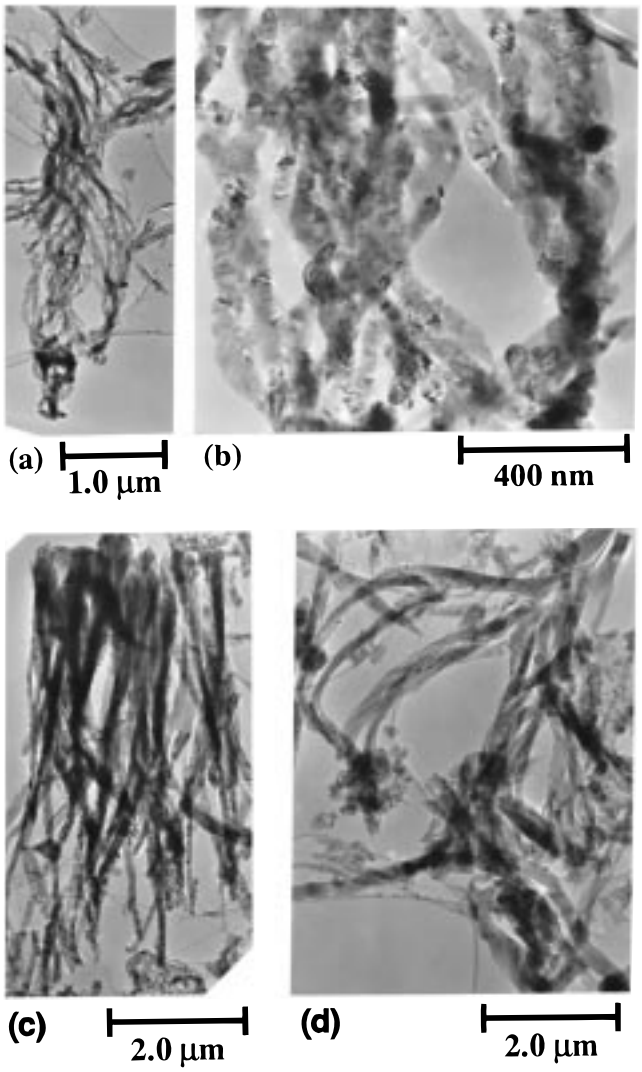

Figure 6. Fibrous and equiaxed AlN morphologies obtained upon Al nitridation using rapid heating rates in the presence of added $AlCl_3$. (a and b) Two magnifications revealing the polycrystallinity of the fibers. (c) A hairlike bundle along with aggregates of equiaxed particles. (d) Split and curved fibers along with aggregates of equiaxed particles, which resembles the hair on partially reacted droplets (Figure 7b).

coalesced into larger droplets, which were also larger than the sizes of the equiaxed AlN product particles that grew upon them (see below). Thus, the sizes of the equiaxed AlN particles were not directly determined by the initial Al particle sizes. Faster heating rates resulted in smaller increases in the Al particle sizes, supporting the observation above of faster heating rates giving larger nanowhisker fractions. Smaller increases in the sizes of the reacting Al droplets maintained a higher effective surface area for Al evaporation or interfacial reaction with $AlCl_3$ (see the Discussion section).

Addition of $AlCl_3$ greatly altered the morphologies of the partially reacted eq-2 and 2-μm Al. With no $AlCl_3$ added, the partially reacted particles were spheroidal and covered with short AlN stubble (Figure 7a). When $AlCl_3$ was added, two types of partially reacted particles were observed, spheroids with long AlN hair (Figure 7b) and smaller starfishlike particles having a dense AlN coating (Figure 7c). In addition, samples to which $AlCl_3$ had been added contained spheroids with cracks and holes, which revealed hollow interiors (Figure 8). These

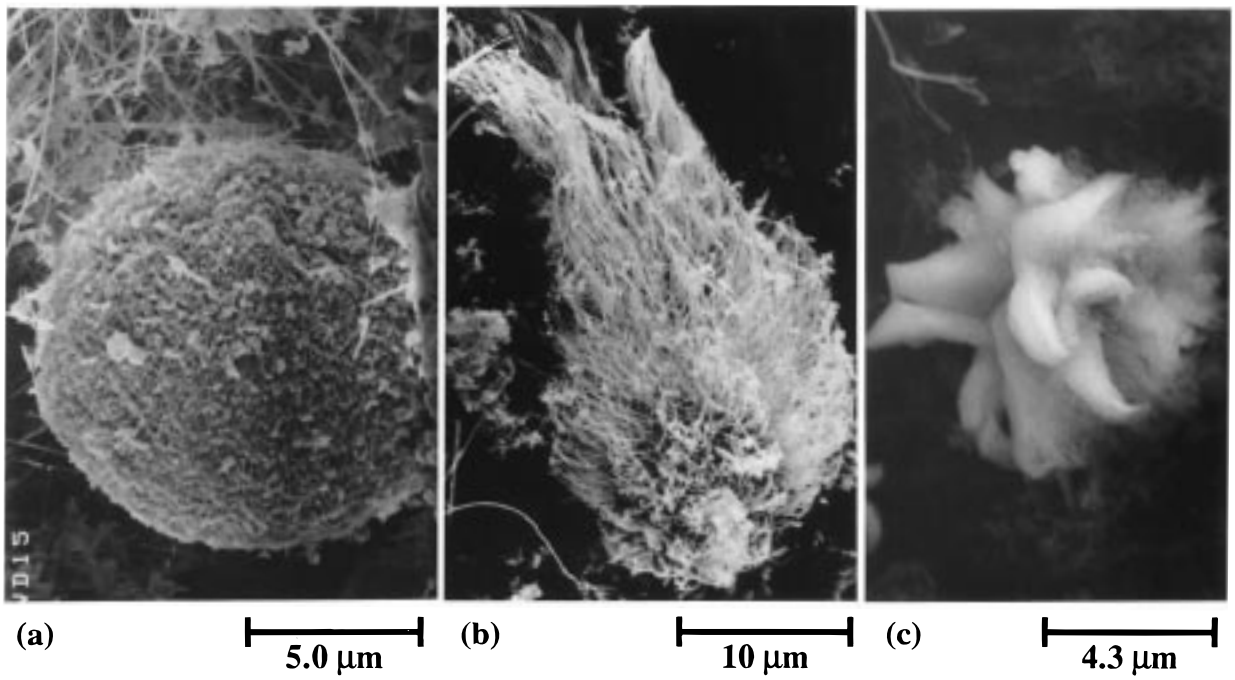

Figure 7. Partially reacted (nitrided) Al droplets: (a) without added $AlCl_3$ (note the coating of AlN stubble), (b) with added $AlCl_3$ (note hairlike AlN deposit), and (c) with added $AlCl_3$ (note the starlike particle with a dense AlN coating).

hollow particles were observed for all of the starting Al powders, but only when $AlCl_3$ was added. The results suggested that reacting Al droplets became coated with a shell of AlN stubble or hair and that Al was subsequently transported from the interior of the spheroids by action of $AlCl_3$, hollowing them.

The AlN stubble and hair coating the partially reacted Al droplets appeared to be fibrous aggregates of small particles. The SEM images did not firmly establish these structures to be dense polycrystalline fibers. However, the appearance of the stubble and hair closely resembled the twisted, polycrystalline fibers produced under conditions of highest effective Al vapor pressure (Figure 6), suggesting they were similarly constituted. In contrast, the nanowhiskers appeared to grow at sites separated from the coated Al droplets.

The results may be summarized as follows. Fine Al powders and N_2 reacted at 900−1100 °C to give nanocrystalline AlN; these nitridation reactions went to completion only when the initial Al particle sizes were in the nanometer size regime. The AlN nanoparticles were formed primarily in equiaxed or nanowhisker morphologies. The additive $AlCl_3$ was a nanowhisker-growth promoter. Impurities in the starting Al were concentrated in the equiaxed AlN particles. Conditions that enhanced the rate of Al evaporation or interfacial reaction with $AlCl_3$ increased the nanowhisker fraction. The Al particles in the starting powders were found to coalesce into larger droplets under nitridation conditions and to become coated with a shell of polycrystalline AlN. When $AlCl_3$ was added, these AlN-coated droplets became hollowed out. The single-crystal AlN nanowhiskers grew separately from the AlN-coated Al droplets. The results were consistent with a growth model in which the equiaxed AlN nanoparticles precipitated at or near the surface of the coalesced Al droplets, whereas the AlN nanowhiskers grew apart from the Al droplets in a vapor-transport process mediated by $AlCl_3$.

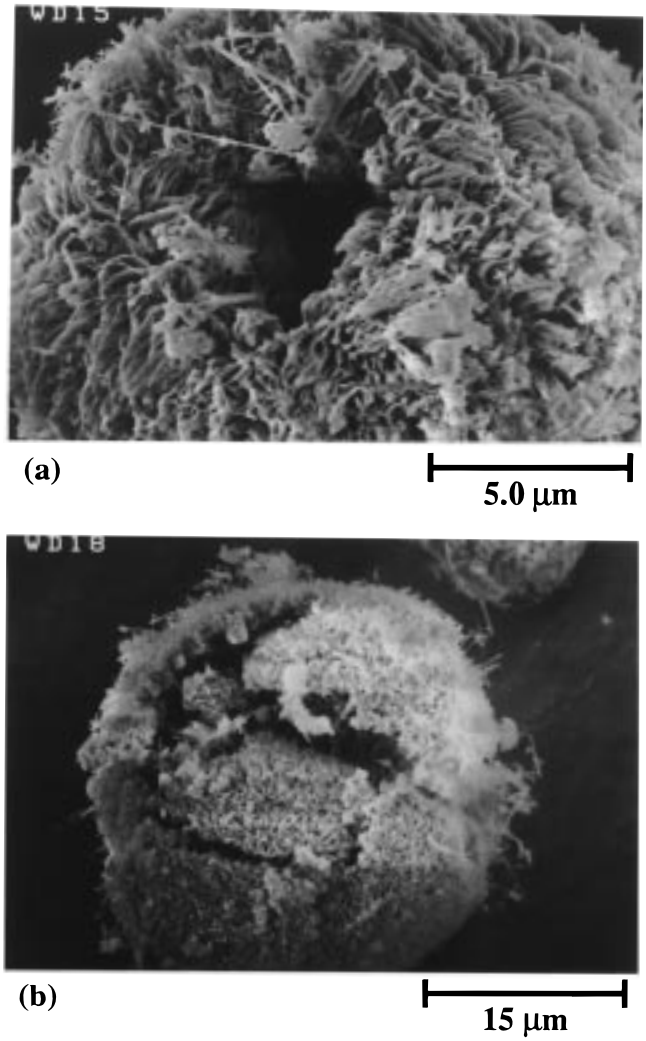

Figure 8. Hollowed AlN shells produced by nitridation of (a) eq-2 nano-Al with $AlCl_3$ added and (b) 20-μm Al with $AlCl_3$ added.

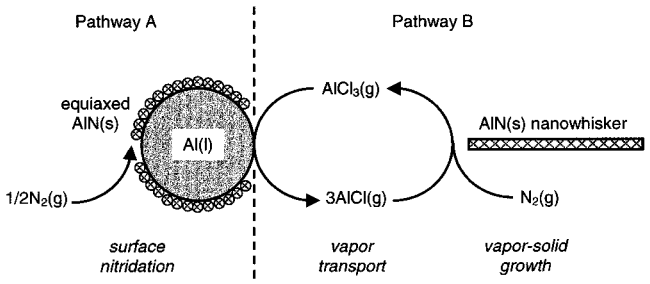

Figure 9. Proposed dominant reaction pathways A and B for nitridation of Al.

Discussion

We propose that the nano-AlN morphological selectivity is established by the relative contributions of the two reaction pathways shown in Figure 9. Use of commercial or eq-2 Al powders, larger Al particle sizes, and slower heating rates favor pathway A and produce distributions weighted toward equiaxed nanocrystallites. Use of eq-1 Al or added $AlCl_3$, smaller Al particle sizes, and faster heating rates favor pathway B and produce distributions weighted toward nanowhiskers. As described above, under appropriate conditions high specificities for equiaxed or nanowhisker morphologies are achieved. The proposed pathways A and B, the proposed vapor−solid nanowhisker growth mechanism, the role of $AlCl_3$, and the extent of Al conversion are discussed below. Precedent established that nitridation of liquid and gaseous Al was expected to produce the differing morphologies observed here.

Nitridation of liquid Al has been previously shown to produce microstructures such as those in Figures 7a and 8, as we propose in pathway A (Figure 9). Hotta et al.[39,40] reported that Al(l) and N_2 react at 1350−1550 °C to give hollow, spherical, 4−12-μm AlN aggregates of 0.1−0.2-μm equiaxed particles. Chang et al.[41] found that 8-μm starting Al powder was converted with N_2 or N_2/NH_3 at 1000−1300 °C by the floating nitridation method to cracked or porous, spherical aggregates of nano-AlN. In contrast, when equiaxed AlN particles are produced by vapor-phase reaction of *gaseous* Al[42,43] or organoaluminum precursors,[44] the resulting microstructures are nonagglomerated or only loosely agglomerated.

Our observations of intermediate, partially converted Al/AlN microstructures revealed that the hollow or porous spherical aggregates resulted from Al droplet coalescence followed by AlN precipitation upon the droplet surfaces. Al(l) has a greater thermal-expansion coefficient than does AlN(s).[39,40] Thus, the AlN coatings are fractured as the Al(l) in the interior expands during heating, creating channels into the unreacted interior of the particle through which Al evaporates and N_2 penetrates, creating the observed microstructure (Figures 7a and 8).[42] This conversion mechanism is likely also responsible for the hollow or porous spherical AlN microstructures produced from Al(l) in the prior studies noted above.

The dramatic increase in whisker fraction and formation of hollow AlN shells upon addition of $AlCl_3$ support a mechanism in which $AlCl_3$ acts as a vapor-transport agent. $AlCl_3$(g) and Al(l) are known to form significant equilibrium quantities of AlCl(g) and $AlCl_2$(g) at the nitridation temperatures employed.[45,46] Moreover, AlCl and $AlCl_2$ react with N_2, whereas $AlCl_3$ does not.[46] We propose that AlCl(g) or $AlCl_2$(g) are the volatile Al carriers that increase the effective Al vapor pressure and enable the growth of nanowhiskers, platelets, and other faceted morphologies at moderate temperatures (pathway B, Figure 9). In our reactor, generation of the Al subchlorides competes with sublimation of $AlCl_3$ out of the furnace. Thus, rapid heating rates increase the whisker fraction in part by decreasing the amount of $AlCl_3$ subliming out of the hot zone before nitridation temperatures are reached.

We propose pathway B (Figure 9) to be a vapor−solid (VS) growth mechanism in which the AlN nanowhiskers grow directly from gaseous nutrient species (aluminum subchlorides). Both VS and vapor−liquid−solid (VLS) mechanisms must be considered, because AlN whiskers have been grown by both mechanisms.[34,35,47] In the VLS mechanism whiskers grow from liquid flux droplets attached to whisker tips.[48,49] We observed no flux droplets, and addition of various potential flux materials (LiCl, LiO_2, $LiAlO_2$, and $LiAl_5O_8$) did not promote whisker formation.[48,49] Additionally, the variety of observed crystallite morphologies and whisker-growth directions is more consistent with VS growth than it is with VLS growth.[48−50] The branched, comblike, and scale-decorated crystallites suggest that addition of large amounts of $AlCl_3$ or rapid heating rates alter the growth kinetics and activate additional growth directions. The unusual morphologies are reminiscent of dendritic growth, which results from nonequilibrium growth conditions, i.e., nutrient-concentration gradients at the growth interface. These changes in growth behavior with alterations in reaction conditions are also more consistent with VS growth than they are with VLS growth.[48−50]

Morphologies of crystallites grown from the vapor phase are known to depend on the degree of supersaturation of the nutrient species. Low supersaturations produce whiskers, higher supersaturations produce platelets, and still higher supersaturations produce equiaxed particles.[50,51] Nitridation of Al(l) at ≥1400 °C or carbothermal reduction at ≥1800 °C often produces AlN whiskers. AlN whiskers grow on the reaction-

(39) Hotta, N.; Kimura, I.; Ichiya, K.; Saito, N.; Yasukawa, S.; Tada, K.; Kitamura, T. *J. Ceram. Soc. Jpn., Int. Ed.* **1988**, *96*, 715−719 (*Nippon Seramikkusu Kyokai Gakujutsu Ronbunshi*, **1988**, *96*, 731−735).
(40) Hotta, N.; Kimura, I.; Tsukuno, A.; Saito, N.; Matsuo, S. *J. Ceram. Soc. Jpn., Inter. Ed.* **1987**, *95*, 246−248 (*Yogyo Kyokaishi*, **1987**, *95*, 274−278).
(41) Chang, A.-J.; Rhee, S.-W.; Baik, S. *J. Mater. Sci.* **1995**, *30*, 1180−1186.
(42) Pratsinis, S. E.; Wang, G.; Panda, S.; Guiton, T.; Weimer, A. *J. Mater. Res.* **1995**, *10*, 512−520.
(43) Johnston, G. P.; Muenchausen, R. E.; Smith, D. M.; Foltyn, S. R.*J. Am. Ceram. Soc.* **1992**, *75*, 3465−68.
(44) Adjaottor, A. A.; Griffin, G. L. *J. Am. Ceram. Soc.* **1992**, *75*, 3209−14.
(45) Roa, D. B.; Dadape, V. V. *J. Phys. Chem.* **1966**, *70*, 1349−1353.
(46) Nickel, K. G.; Riedel, R.; Petzow, G. *J. Am. Ceram. Soc.* **1989**, *72*, 1804−1810.
(47) Miao, W.-G.; Wu, Y.; Zhou, H.-P. *J. Mater. Sci.* **1997**, *32*, 1969−1975.
(48) Givargizov, E. I. In *Current Topics in Materials Science*; Kaldis, E., Ed.; North-Holland Publishing: New York, 1978; Vol. 1, p 22.
(49) Givargizov. E. I. *J. Cryst. Growth* **1975**, *31*, 320−30.
(50) Campbell, W. B. In *Whisker Technology*; Levitt, A. P., Ed.; Wiley-Interscience: New York, 1970; pp 17, 27, and 28.
(51) Loper, C. R. Jr.; Rasmussen, D. H.; Koelling, H. A. *J. Cryst. Growth* **1971**, *9*, 2117−227.

vessel walls during floating nitridation of Al.[12,39,40] The carbothermal-reduction process has been used to grow AlN whiskers intentionally[35,47] and also produces whisker deposits downstream from the sample where equiaxed particles form.[52] Whiskers are grown at lower temperatures using volatile Al species as the Al sources; for example, whiskers are grown at 900 °C using $AlBr_3$.[33] Thus, high temperatures are typically required to produce sufficient Al(g) from Al(l) to support whisker growth, whereas lower temperatures are required for whisker growth from volatile Al compounds.

We suggest that the fibrous deposits observed on the spheroids in some partially reacted samples (Figure 7b) result from a microscopic version of the morphological influences operating in the carbothermal-reduction study noted above.[52] The fibrous hair on the spheroids is polycrystalline and sometimes resembles chains of equiaxed particles (Figures 6a,b). The growth of these microstructures may be due to larger gaseous Al−nutrient concentrations immediately adjacent to the cracks in the AlN shells on the spheroids from which the nutrient species emerge. Equiaxed AlN grains are presumably sequentially deposited upon one another at these maximum nutrient concentrations to produce the fibrous, polycrystalline microstructures. At sites remote from the coated spheroids, the Al−nutrient concentrations are lower and support the growth of nanowhiskers. Our observations parallel the upstream and downstream growth of equiaxed and whisker particles, respectively, found in the carbothermal-reduction synthesis of AlN.[52]

The results also suggest that the starting Al particle sizes influence the effective Al vapor pressure and, hence, the morphological distribution in the AlN product. An increase in the equilibrium vapor pressure is expected for particle sizes in the nanometer regime, as is revealed by the Kelvin equation.[53] However, the Kelvin equation predicts a vapor-pressure increase of at most 2−3% for the particle-size distributions of the nano-Al used here (and obtained from eqs 1 or 2). Consequently, the large nanowhisker fractions produced at comparatively low temperatures in the present work cannot be ascribed to such an equilibrium effect, and we look for a likely kinetic effect. We surmise that the large surface areas of the nano-Al powders lead to increased rates of Al evaporation or increased rates of interfacial reaction of Al(s) and $AlCl_3$, producing large steady-state concentrations of gaseous Al−nutrient species.

We find that nano-Al (from eqs 1 and 2) reacts completely at the mild nitridation temperatures of 900−1100 °C. In contrast, the industrial direct-nitridation and carbothermal-reduction processes using larger Al particles require reaction temperatures of ≥1500 and 1700−1800 °C, respectively, and intermediate grinding to achieve complete reaction.[3,5] In direct nitridation, the surfaces of large Al droplets become passivated with layers of AlN product, which then hinder complete nitridation. But Al droplets retaining dimensions smaller than the necessary thickness of passivating AlN layers should react completely; the droplets will be completely nitrided before passivating thicknesses are achieved. We presume that the ease of complete nitridation of the nano-Al powders is such a particle-size effect. However, the nitridation may also be aided by the AlN coating present in our reaction tube; AlN particles are frequently added to Al powder before nitridation to improve the conversion effeciency.[12]

Interestingly, addition of $AlCl_3$ to the 2- and 20-μm starting Al powders increases the amount of residual Al in the product. A second kind of passivating layer, an Al_2O_3 layer, is generally present on the surfaces of Al particles. Additives that react with and remove this alumina layer at low temperatures are often mixed with the Al powders in direct nitridation syntheses.[3−5] For example, Li and LiCl activate Al particles and enable complete nitridation at 940−1200 °C.[54,55] The Li-containing compounds react with the Al_2O_3 to form volatile Li_2O, $LiAlO_2$, and $LiAl_5O_8$, which are transported from the AlN product.[55] We surmise that $AlCl_3$ is similarly activating the Al by forming volatile AlO_xCl_y species because lower O levels are found in the AlN when $AlCl_3$ is used. Many of the additives used also produce phases on the surface of the Al droplets that prevent the development of a dense, passivating AlN layer.[4] $AlCl_3$ appears not to hinder the formation of a dense AlN coating, as the partially nitrided Al contains particles with dense AlN coatings. Perhaps $AlCl_3$ assists the formation of dense, passivating AlN layers, accounting for the increased amounts of residual Al.

Conclusions

Morphological selectivity in the growth of nano-AlN is accomplished by varying the relative contributions of competing reaction pathways (Figure 9). Direct surface nitridation of *liquid* Al in the form of small droplets gives primarily equiaxed particles, whereas nitridation of *gaseous* Al species gives primarily nanowhiskers by VS crystal growth. Added $AlCl_3$ functions as a vapor-transport agent that generates volatile, reactive Al subchlorides, which are a nutrient species for nanowhisker growth. The benefit of using nanocrystalline starting Al powders is that complete nitridation is achieved under comparatively mild conditions.

Acknowledgment. This work was funded by NSF grants CHE-9158369 and CHE-9709104, with additional support from the Exxon Education Foundation, Emerson Electric, Monsanto, and Eastman Kodak. J.A.H. was partially supported by a Department of Education GAANN grant (P200A40147). We thank W. L. Gladfelter, T. P. Hanusa, and T. Turney for suggesting the participation of aluminum subchlorides in the VS process.

CM980481+

(52) Forslund, B.; Zheng, J. *J. Mater. Sci.* **1993**, *28*, 3125−3131.
(53) Atkins, P. W. *Physical Chemistry*, 4th ed.; W. H. Freeman: New York, 1990; p 158.
(54) Scholz, H.; Greil, P. *J. Eur. Ceram. Soc.* **1990**, *6*, 237−242.
(55) Haussonne, J. M.; Lostec, J.; Bertot, J. P.; Lostec, L.; Sadou, S. *Am. Ceram. Soc. Bull.* **1993**, *75*, 84−90.